International Journal of Computational Intelligence Systems, Vol.2, No. 3 (October, 2009), 168-183

Anisotropic Wavelet-Based Image Nearness Measure*

James F. PETERS [1] †, Leszek PUZIO [1,2]

[1] *Computational Intelligence Laboratory,*
Electrical & Computer Engineering Department, University of Manitoba
Winnipeg, Manitoba R3T 5V6 Canada
E-mail: jfpeters@ee.umanitoba.ca

[2] *Department of Information Systems and Applications*
University of Information Technology and Management
35-225 Rzeszow, ul. H.Sucharskiego 2, Poland
E-mail: lpuzio@wsiz.rzeszow.pl

Received: 30/04/09
Accepted: 26/06/09

Abstract

The problem considered in this article is how to solve the image correspondence problem in cases where it is important to measure changes in the contour, position, and spatial orientation of bounded regions. This article introduces a computational intelligence approach to the solution of this problem with anisotropic (direction dependent) wavelets and a tolerance near set approach to detecting similarities in pairs of images. Near sets are a recent generalization of rough sets introduced by Z. Pawlak during the early 1980s. Near sets resulted from a study of the perceptual basis for rough sets. Pairs of sets containing objects with similar descriptions are known as near sets. The proposed wavelet-based image nearness measure is compared with F. Hausdorff and P. Mahalanobis image distance measures. The results of three wavelet-based image resemblance measures for several well-known images, are given. A direct benefit of this research is an effective means of grouping together (classifying) images that correspond to each other relative to minuscule similarities in the contour, position, and spatial orientation of bounded regions in the images, especially in videos containing image sequences showing varied object movements. The contribution of this article is the introduction of an anisotropic wavelet-based measure of image resemblance using a near set approach.

Keywords: Anisotropic wavelets, Image resemblance, Near sets, Image nearness measure.

1. Introduction

This paper introduces a wavelet-based near set approach to solving the image correspondence problem, *i.e.*, where one uses anisotropic (direction dependent) wavelets to establish a correspondence between pairs of images. This is one of the central tasks in photogrammetry and computer vision. Recently, it has been shown that near sets can be used in a perception-based approach to discovering correspondences between images [16–19, 39, 41, 42]. Work on a basis for near sets began in 2002, mo-

*Anisotropic Wavelet-Based Image Nearness Measure
†Electrical & Computer Engineering Department, University of Manitoba
Winnipeg, Manitoba R3T 5V6 Canada

tivated by image analysis and inspired by a study of the perception of the nearness of perceptual objects carried out in cooperation with Z. Pawlak in [32]. This initial work led to the introduction of near sets [36], elaborated in [35, 39, 44]. Recently, the study of a perceptual basis for discovering resemblances between images led to a tolerance class form of near sets [39] that models human perception in a physical continuum viewed in the context of image tolerance spaces. A near set-based approach to perceiving image resemblances hearkens back to the observation about perception made by E. Orłowska in 1982 [27] (see, also, [28]), *i.e.*, classes defined in an approximation space serve as a formal counterpart of perception. Sets of perceptual objects where two or more of the objects have similar descriptions are called near sets. For example, sets of images containing bounded regions with similar descriptions are examples of near sets. In particular, consider an image description based on spatial orientation. Let ϕ be a function that measures the spatial orientation of a line segment in an image. Then let $\phi(x), \phi(y)$ denote the spatial orientations of a line segments x, y, respectively, in a pair of images I_x, I_y viewed as sets of line segments. In the case where the L_2 norm $\| \phi(x) - \phi(y) \|_2 \leqslant \varepsilon$, then images I_x, I_y are examples of near sets, *i.e.*, $\| \phi(x) - \phi(y) \|_2 = (\sum_{i=1}^{k} d_i^2)^{\frac{1}{2}} \leqslant \varepsilon$, where $d_i(x_i, y_i)^2 = (\phi(x_i) - \phi(y_i))^2$. In general, $\mathbf{d}^T, \mathbf{d}$ denote row and column vectors containing k feature value differences extracted from a pair of images, respectively, *i.e.*,

$$\mathbf{d}^T = (d_1 \dots d_k), \mathbf{d} = \begin{bmatrix} d_1 \\ \dots \\ d_k \end{bmatrix}. \tag{1}$$

Finally, the overall distance is the L_2 norm $\| \mathbf{d} \|_2$ for a vector $\mathbf{d}$ of feature value differences, *i.e.*,

$$\| \mathbf{d} \|_2 = (\mathbf{d}^T \mathbf{d})^{\frac{1}{2}} = \sqrt{\sum_{i=1}^{k} d_i(x_i, y_i)^2}. \tag{2}$$

Stemming from the work of Henri Lebesgue, $\| \cdot \|_2$ denotes the length of a vector in L_2 space [21]. Spatial orientation of image line segments can be measured with direction-dependent (anisotropic) wavelets. In general, a wavelet is a scaled function that measures waveform variations [25].

The proposed approach to measuring image similarity stems from recent work on anisotropic wavelets [46–48], image correspondence [13, 16, 18, 37, 39] and near sets [16, 26, 34–37, 39, 44]. Similarities between images can be measured by taking into account image features such as contour, spatial orientation and position of line segments along bounded regions contained in sample images. Each image feature is represented by what is known as a probe function, a partial model of perception viewed as a mapping $\phi : X \rightarrow \Re$ inspired by a psychophysics interpretation of the relation between a set of stimuli X and sensation [1]. The notion of an image probe function was first introduced in 1993 by M. Pavel as part of a study of image registration [29] and later refined in [16]. The basic idea is to "probe" images as part of a feature-extraction process. Feature extraction is a well-travelled and yet still a very active research area, *e.g.*, [5, 8, 20, 22, 51]. The proposed near set approach to image classification (*i.e.*, detecting images that correspond to each other) is also akin to the approach to video classification by M.K. Geetha and S. Palanivel [10]. The proposed use of anisotropic wavelets relative to the contour of images in the study of image correspondence also has some kinship with recent work by V. De Witte, S. Schulte and E.K. Kerre [57] on morphological image interpolation in magnifying colour images with sharp edges. A direct benefit of this research is an effective means of grouping together (classifying) images that correspond to each other relative to minuscule similarities in the contour, position, and spatial orientation of bounded regions in the images, especially in videos containing image sequences showing varied object movements (see, *e.g.*, [15, 16, 40, 42, 44]). The contribution of this article is the introduction of an anisotropic wavelet-based measure of image resemblance using a near set approach.

This paper has the following organization. Sect. 2 presents the basics for anisotropic wavelets. A tolerance space and a tolerance nearness measure are presented and illustrated in Sect. 3. Image nearness measurement results are reported in Sect. 4. Hausdorff and Mahalanobis distance measures are briefly presented in Sect. 5. A comparison of the results using all three image resemblance measures is given in Sect. 6.

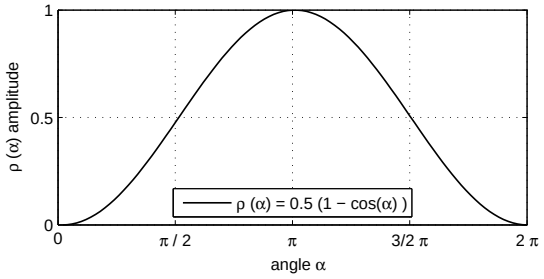

1.1: Single Hann window

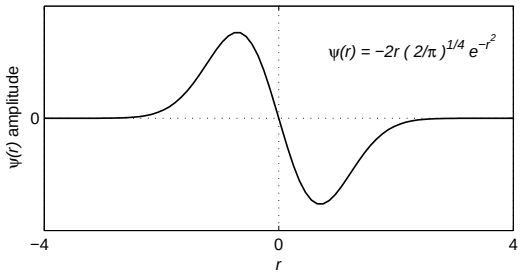

1.2: Single Gaussian wavelet

Fig. 1. Hann Window and Gaussian Wavelet

2. Anisotropic Wavelets

An anisotropic wavelet (*i.e.*, dependent on the direction (angle) that is used to define a wavelet) is constructed in a polar coordinate system as a product of the Hann window function and the Gaussian wavelet [47]. The Hann window function is given in (3). Figure 1.1 presents a single Hann window function constructed using (3). The Gaussian wavelet is given in (4). Figure 1.2 presents a single Gaussian wavelet.

$$\rho(\alpha) = 0.5(1-\cos(\alpha)),\ \alpha \in [0, 2\pi), \tag{3}$$

$$\psi(r) = -2r\left(\frac{2}{\pi}\right)^{1/4} e^{-r^2}. \tag{4}$$

An anisotropic wavelet $\psi(\alpha, r)$ is a product of a Hann window $\rho(\alpha)$ and translated by n_r Gaussian wavelet $\psi(r)$ represented in (5). By putting (3) and (4) into (5), we obtain a so-called 'mother wavelet', *i.e.*, a wavelet function (6) that is used to construct a wavelet set. Other approaches to wavelet construction with different spatial orientations are given in [25] and [2–4,56]. Using (6), we construct a wavelet set. Each wavelet in our set we calculate in (7).

$$\psi(\alpha, r) = \rho(\alpha)\psi(r), \tag{5}$$

$$\psi(\alpha, r) = 0.5(1-\cos(\alpha))\ (-2r)\left(\frac{2}{\pi}\right)^{1/4} e^{-r^2}, \tag{6}$$

$$\psi_{\mathscr{I}}(\alpha, r) = \tag{7}$$

$$\left(1/\sqrt{2\pi n_r/2^{s_\alpha+1}}\sqrt{2^{-s_r}}\right)\cdot \tag{8}$$

$$\psi\left(2^{s_\alpha}\alpha - \pi(n_\alpha - 1), 2^{-s_r}(r - n_r)\right), \tag{9}$$

$$C_\psi\{f\}(\dots) = \int\int f(\alpha, r)\psi^*_{s_\alpha, s_r, n_\alpha, n_r}(\alpha, r)\, d\alpha\, dr. \tag{10}$$

where $C_\psi\{f\}(\dots)$ denotes $C_\psi\{f\}(s_\alpha, s_r, n_\alpha, n_r)$, ψ denotes a wavelet with (α, r) a polar coordinates and where $\mathscr{I} = \{s_\alpha, s_r, n_\alpha, n_r\}$ denotes an index set used in (7) to define a wavelet with an angular scale s_α, radial scale s_r, an angular translation n_α and a radial translation n_r. In particular, it is n_α that makes (7) anisotropic, while n_r is a radial distance from the pole (origin of a polar coordinate system). For the sake of clarity, we sometimes write $\psi_{s_\alpha, s_r, n_\alpha, n_r}(\alpha, r)$ rather than the more concise $\psi_{\mathscr{I}}(\alpha, r)$ (see, *e.g.*, (10)).

We use the wavelet set in Fig. 3.1 to calculate wavelet coefficients (which are real numbers) given in (10), where C denotes a wavelet coefficient and $f(\alpha, r)$ is a function in polar coordinate that describes image values. Using (10), we calculate wavelet coefficients. Than we choose a wavelet with coefficient maximum value. If the coefficient

maximum value is greater than the threshold (for the threshold, we use 15% of the maximum coefficient value), then we assume that we found an edge. Therefore, our probe function for a given point of an image gives two features. The first feature is a wavelet coefficient value which corresponds to edge intensity change and the second feature is a wavelet orientation that corresponds to edge spatial orientation.

The angular scale s_α determines how many wavelets we have in a wavelet set. Wavelet set number is equal to $2^{s_\alpha+1}$. We assumed in (7) $s_\alpha = 3$; therefore each wavelet set consists of 16 wavelets. To construct a wavelet set, we used $s_r = 0,1,2,3,4$ values. A greater s_r value gives wavelets with greater support, *i.e.*, a set of points where a wavelet is not zero. In our implementation, we assumed that the wavelet support is a set of points with value greater than 0.001, since a Gaussian wavelet used in our wavelet construction has infinitive support. Table 1 shows wavelet support width dependency (along r coordinate) on scale s_r. Figure 2 presents a single wavelet obtained using (7). Every wavelet in a set has the same scale s_r but different spatial orientation n_α in the image plane. Figure 3.1 presents wavelets with different spatial orientation. Wavelets have different spatial orientation because of different angular translation n_α. Wavelets in Figure 3.1 in the left-upper corner have angular translation $n_\alpha = 0,1,2,3,4,5,6,7,8$. This wavelet set is able to detect edges at given points of an image and estimate its spatial orientation [48] or may be used for particular points detection [47].

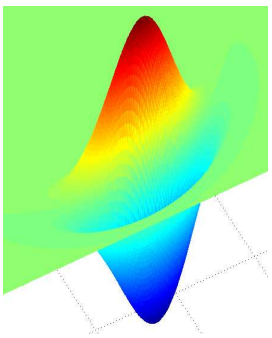

2.1: 3D wavelet

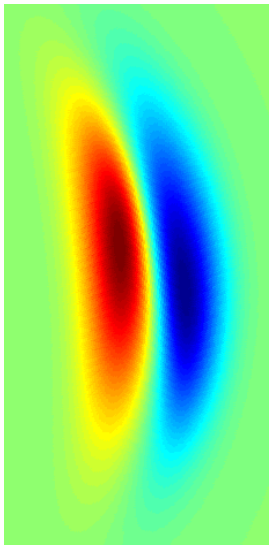

2.2: 2D wavelet

Fig. 2. Sample Wavelets

Table 1. support vs. s_r scale.

s_r scale	support width [px]
0	5
1	9
2	17
3	33
4	65

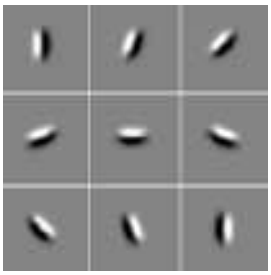

3.1: $s_\alpha = 3, s_r = 3$

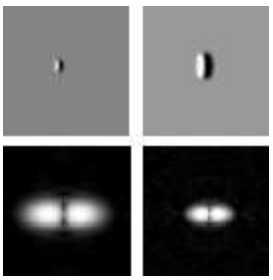

3.2: s_r=1 (left), s_r=2 (right)

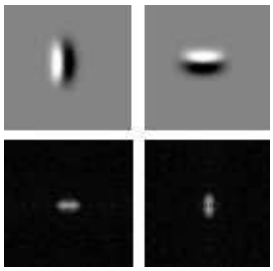

3.3: s_r=3, n_α=0 (left) and n_α=4 (right)

Fig. 3. Sample Wavelet Sets

The presented wavelet has multi-resolution and anisotropic properties. Fig. 3.2 shows that a wavelet with scale $s_r = 1$ has higher spatial frequencies than a wavelet with scale $s_r = 2$. Therefore, this wavelet set can be used as a multi-resolution filter bank. Figure 3.3 presents two wavelets in the same scale and with different spatial orientation. The top left wavelet has orientation $n_\alpha = 0$ and the top right wavelet has $n_\alpha = 4$. Wavelet Fourier transforms prove that they have different spatial orientations (the difference equals to 90 degrees).

3. Tolerance Space for Image Recognition

A perception-based approach to discovering resemblances between images leads to a tolerance class form of near sets that models human perception in a physical continuum viewed in the context of image tolerance spaces. A tolerance space-based approach to perceiving image resemblances hearkens back to the observation about perception made by Ewa Orłowska in 1982 [27] (see, also, [28]), *i.e.*, classes defined in an approximation space serve as a formal counterpart of perception.

The term *tolerance space* was coined by E.C. Zeeman in 1961 in modelling visual perception with tolerances [58]. A tolerance space is a set X supplied with a binary relation $\simeq$ (*i.e.*, a subset $\simeq \subset X \times X$) that is reflexive (for all $x \in X$, $x \simeq x$) and symmetric (for all $x, y \in X$, $x \simeq y$ and $x \simeq y$) but transitivity of $\simeq$ is not required. For example, it is possible to define a tolerance space relative to subimages of an image. This is made possible by assuming that each image is a set of fixed points. Let O denote a set of perceptual objects (*e.g.*, grey level subimages) and let $gr(x)$ = average grey level of subimage x. Then the tolerance relation $\simeq_{gr}$ is defined as

$$\simeq_{gr} = \{(x,y) \in O \times O \mid |gr(x) - gr(y)| \leqslant \varepsilon\},$$

for some tolerance $\varepsilon \in \Re$ (reals). Then $(O, \simeq_{gr})$ is a sample tolerance space. A tolerance denoted by ε is directly related to the exact idea of closeness or resemblance (*i.e.*, being within some tolerance) in comparing objects. The basic idea is to find objects such as images that resemble each other with a tolerable level of error. A. Sossinsky [55] observes that main idea underlying tolerance theory comes from H. Poincaré [45]. Physical continua (*e.g.*, measurable magnitudes in the physical world of medical imaging [13]) are contrasted with the mathematical continua (real numbers) where almost solutions are common and a given equation have no exact solutions. An *almost solution* of an equation (or a system of equations) is an object which, when substituted into the equation, transforms it into a numerical 'almost identity', *i.e.*, a relation between numbers which is true only approximately (within a prescribed tolerance) [55]. Equality in the physical world is meaningless, since it can never be verified either in practice or in theory. Hence, the basic idea in a tolerance space view of images, for example, is to replace the indiscernibility relation in rough sets [31] with a tolerance relation in partitioning images into homologous regions where there is a high likelihood of overlaps, *i.e.*, non-empty intersections between image tolerance classes. The use of image tolerance spaces in

this work is directly linked to recent work on tolerance spaces [9, 11, 13, 38, 39, 43, 52–54, 59]. The contribution of this article is the introduction of two new tolerance space-based image resemblance measures and a comparison of the new measures with the original Henry-Peters nearness measure.

When dealing with perceptual objects (especially, components in images), it is sometimes necessary to relax the equivalence condition in the original indiscernibility relation introduced by Z. Pawlak [31, 33] to facilitate observation of associations in a perceptual system. This variation is called a tolerance relation that defines yet another form of near sets [38, 39, 43] and is given in Def. 1. A perceptual tolerance relation is defined in the context of perceptual systems in (11).

Definition 1 Perceptual Tolerance Relation [43] Let $\langle O, \mathbb{F} \rangle$ be a perceptual system and let $\varepsilon \in \Re$ (set of all real numbers). For every $\mathscr{B} \subseteq \mathbb{F}$ the perceptual tolerance relation $\simeq_{\mathscr{B},\varepsilon}$ is defined in (11).

$$\simeq_{\mathscr{B},\varepsilon} = \{(x,y) \in O \times O \mid \| \phi(x) - \phi(y) \|_2 \leqslant \varepsilon\}, \tag{11}$$

where $\| \cdot \|_2$ is the L_2 norm, $\phi(x) = [\phi_1(x)\ \phi_2(x)\ ...\ \phi_l(x)]^T$ is a feature-value vector obtained using all the probe functions in $\mathscr{B}$. A probe function is a real-valued function representing features of physical objects.
Notice that if $\varepsilon = 0$, then $\simeq_{\mathscr{B},\varepsilon}$ is an equivalence relation similar to the original indiscernibility relation introduced by Z. Pawlak in 1981-1982 [30, 31], *i.e.*,

$$\simeq_{\mathscr{B},0} = \{(x,y) \in O \times O \mid \| \phi(x) - \phi(y) \|_2 = 0\}$$

The relation $\simeq_{\mathscr{B},0}$ is useful, since it defines a partition (segmentation) of an image (this was pointed out in [13, 18]).

4.1: Lena

4.2: Lena Tol. Classes

4.3: Lena Eye Classes

4.4: Barbara

4.5: Barb Tol. Classes

4.6: Barb Eye Classes

Fig. 4. Image tolerance classes

Example 1 Grey-Level Tolerance Classes
Let $I1, I2$ denote the pair of images in Fig. 4.1, Fig. 4.4, respectively. The tolerance class coverings for $I1, I2$ are shown in Fig. 4.2,Fig. 4.5, respectively and selected overlapping tolerance classes relative to a particular image region (Fig. 4.3,Fig. 4.6). Let $\langle O, \mathbb{F} \rangle$ be a perceptual system where O denotes the set of 25×25 subimages. The image is di-

vided into 100 subimages of size 25×25 and can be shown as a set $X = O$ of all the 100 subimages. Let $\mathscr{B} = \{\phi_1(x)\} \subseteq \mathbb{F}$ where $\phi_1(x) = gr(x)$ is the average grey scale value of subimage x between 0 and 255. Let $\varepsilon = 25.5(10\%)$. Notice the ■ (very dark) subimages x in the archway in Fig. 4.2 and subimages y in the bookcase (upper left corner) in Fig. 4.5, *i.e.*, subimages x, y have similar grey levels. This reveals that there is at least one tolerance class consisting of subimages extracted from each of the original images. In effect, $x \simeq_{\{gr\},25.5} y$. In fact, it is also the case that $I1 \simeq_{\{gr\},25.5} I2$. To see this, let $I1, I2 \subseteq O$, *i.e.*, $I1, I2$ are viewed as sets of subimages in O. In particular,

$$\simeq_{\phi,25.5} = \{(x,y) \in O \times O \mid \| \phi(x) - \phi(y) \|_2 \leqslant 25.5\}.$$

Also observe, for example, the sample overlapping tolerance classes in Fig. 4.3 containing subimages that include Lena's left eye. Again, for example, observe the sample overlapping tolerance classes in Fig. 4.6 containing subimages that include Barbara's left eye. Relative to the subimage containing Lena's eye and Barbara's eye, each tolerance class contains subimages where the difference between average grey scale values of the subimages are within the prescribed tolerance level ε. In Sect. 3.1, separate image tolerance class coverings for each image provide a basis for measuring the degree that pairs of image resemble each other.

5.1: Lena with ◄

5.2: Edge Tol. Classes

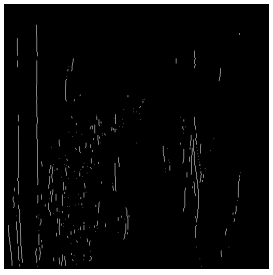

5.3: Lena◄ Edge Class

5.4: Barbara with ◄

5.5: Edge Tol. Classes

5.6: Barb◄ Edge Class

Fig. 5. Orientation tolerance classes

Example 2 Wavelet Orientation Tolerance Classes

Let $I1, I2$ denote the pair of images in Fig. 5.1, Fig. 5.4, respectively. For this example, $s_r = 1$ and $\varepsilon = 0.1$. The wavelet orientation tolerance class coverings for $I1, I2$ are shown in Fig. 5.2, Fig. 5.5, respectively and selected overlapping anisotropic wavelet orientation tolerance classes relative to a particular image edges are shown in (Fig. 5.3, Fig. 5.6). That is, using anisotropic wavelets, a covering of the images consisting of orientation tolerance classes containing edges with similar orientation is shown for each of the original images.

For visualization purposes, a ◄ is pointing to the

selection of an edge belonging to a particular tolerance class, *i.e.*, all edges (tiny line segments) that are close to vertical in both images (with tolerance $\varepsilon = 11.25$ degrees).

3.1. Tolerance Nearness Measure

This section briefly introduces a $L2$ norm-based tolerance nearness measure useful is discerning resemblances between images [15, 38, 39, 43]. Sets can be considered near each other when they have "things" in common. In the context of near sets, the "things" can be quantified by granules of a perceptual system, *i.e.*, the elementary sets. The simplest example of nearness between sets sharing "things" in common is the case when two sets have similar elements. In particular, digital images are viewed as sets of points with definable coverings using Def. 1 and susceptible to comparisons using nearness measures such as the one in (12). This idea leads to the definition of a tolerance nearness relation.

Definition 2 Tolerance Nearness Relation [43]
Let $\langle O, \mathbb{F} \rangle$ be a perceptual system and let $X, Y \subseteq O$. A set X is perceptually near a Y *within* the perceptual system $\langle O, \mathbb{F} \rangle$ (*i.e.*, $(X \underset{\cong}{\bowtie}_{\mathbb{F}} Y)$) iff there are $x \in X$ and $y \in Y$ and there is $\mathscr{B} \subseteq \mathbb{F}$ such that $x \cong_{\mathscr{B},\varepsilon} y$. We then say that X, Y are *perceptually near* each other in the tolerance sense of nearness in Def. 1.
For simplicity, we usually write $x \cong_{\mathscr{B}} y$ instead of $x \cong_{\mathscr{B},\varepsilon} y$. An example of Def. 2 is given in Fig. 6 where the grey lines belong to tolerance classes. The sets X and Y are examples of tolerance near sets in Fig. 6 because they both share objects belonging to the same tolerance class, namely, α.

Defn. 2 can be used to define a Nearness Measure (NM) between two sets X and Y [13, 16]. Let $Z = X \cup Y$ and let the notation

$$[z_{/\cong_{\mathscr{B}}}]_X = \{z \in z_{/\cong_{\mathscr{B}}} \mid z \in X\},$$

denote the portion of the elementary set $z_{/\cong_{\mathscr{B}}}$ that belongs to X, and similarly, use the notation

$$[z_{/\cong_{\mathscr{B}}}]_Y = \{z \in z_{/\cong_{\mathscr{B}}} \mid z \in Y\},$$

to denote the portion that belongs to Y. Further, let the sets X and Y be weakly near each other using Defn. 2. Then, a $NM_{\cong_{\mathscr{B}}}(X,Y)$ between X and Y is given in [15] by (12).

$$NM_{\cong_{\mathscr{B}}}(X,Y) = \frac{\sum_{z_{/\cong_{\mathscr{B}}} \in Z_{/\cong_{\mathscr{B}}}} |z_{/\cong_{\mathscr{B}}}| \frac{\min(|[z_{/\cong_{\mathscr{B}}}]_X|, |[z_{/\cong_{\mathscr{B}}}]_Y|)}{\max(|[z_{/\cong_{\mathscr{B}}}]_X|, |[z_{/\cong_{\mathscr{B}}}]_Y|)}}{\sum_{z_{/\cong_{\mathscr{B}}} \in Z_{/\cong_{\mathscr{B}}}} |z_{/\cong_{\mathscr{B}}}|} \tag{12}$$

The idea behind (12) is that sets that are similar should have a similar number of objects in each tolerance class. Thus, for each tolerance class obtained from $Z = X \cup Y$, (12) counts the number of objects that belong to X and Y and takes the ratio (as a proper fraction) of their cardinalities. Furthermore, each ratio is weighted by the total size of the tolerance class (thus giving importance to the larger classes) and the final result is normalized by dividing by the sum of all the cardinalities. The range of (12) is in the interval [0,1], where a value of 1 is obtained if the sets are equivalent and a value of 0 is obtained if they have no elements in common.

As an example of the degree of nearness between two sets, consider Fig. 7 in which each image consists of two sets of objects, X and Y. Each colour in the figures corresponds to an elementary set where all the objects in the class share the same description. The idea behind Eq. 12 is that the nearness of sets in a perceptual system is based on the cardinality of equivalence classes that they share. Thus, the sets in Fig. 7.1 are closer (more near) to each other in terms of their descriptions than the sets in Fig. 7.2.

4. Image Nearness Measurement Results

This section briefly presents the result of NMs using different features such as wavelet coefficient, wavelet localization, and wavelet orientation or contour length. Contour length is defined as the number of edges that belong to a given contour. In the examples in the sequel, we use all of those features to calculate $NM_{\cong_{\mathscr{B}}}(X,Y)$ (12) relative to pairs of images X and Y. Notice that the images in Figure 8

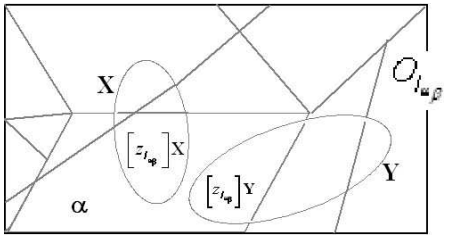

Fig. 6. Example of Defn. 2.

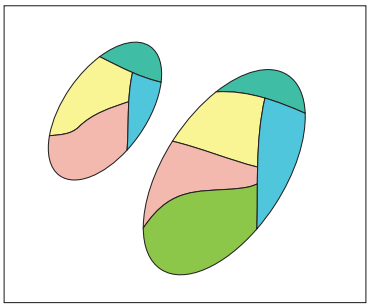

7.1: High nearness

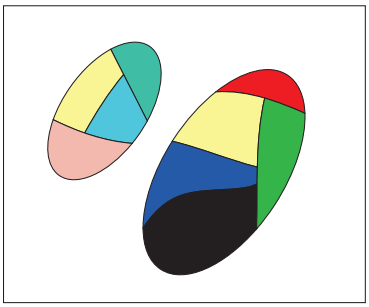

7.2: Low nearness

Fig. 7. Examples of degree of nearness.

have the same average gray level value. Thanks to the edge orientation feature, we are able to distinguish these two images. Table 2 presents nearness measurements. To calculate $NM_{\cong_{\mathscr{B}}}(X,Y)$, we used image features obtained for different s_r scales 4, 3, 2, 1 and 0.

4.2. Portrait Comparison

Figure 9 presents images used for $NM_{\cong_{\mathscr{B}}}(X,Y)$ comparison. Let B,L,M denote the portrait of Barbara, Lena and the Mona Lisa, respectively.

4.2.1. B & L Image Portrait Comparison

Table 3 shows calculated NMs for images B & L. NMs in column entitled 'coefficient' uses wavelet coefficient as a feature and an equation (12) with tolerance ε=0.1. Column entitled 'orientation' uses wavelet orientation as a feature and (12)with tolerance ε=1. Epsilon value equal to 1 means that tolerance is set to $+/-22.5^o$ degrees. The Column entitled 'contour' presents results obtained using contour length as a feature and (12) with tolerance ε=10 of contour points. Obtained NM values are higher, when we use as a feature wavelet coefficient values, when we compare only orientations we get lower NM values. NM with weights gives even lower values. But lowest values of NM gives contours. Table 4 presents NMs of B & L images calculated using (12) and wavelet coefficient values as a feature. Results show that higher epsilon values lead to higher NMs values. It reflects ours expectations, that bigger tolerance leads to bigger nearness of two images. One would expect that with tolerance equal to 1 NM value should be equal to 1, but we have to remember that NM takes into account also tolerance classes number in each images. Table 5 presents NMs of B & L images calculated using equation (12) and contour length as a feature. The epsilon value equal to 1 means that tolerance is set to the maximum contour length value. Figure 10.2 presents NM dependences on epsilon value and wavelet scale. Figure 10.3 shows how the NM based on orientation de-

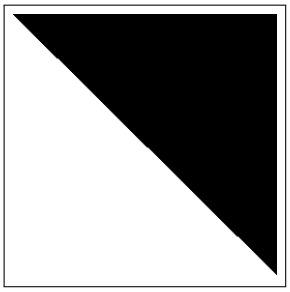

8.1: Lena with ◄

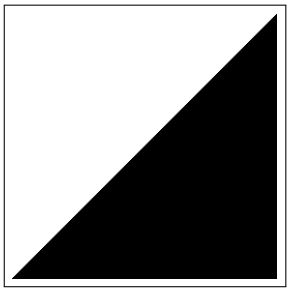

8.2: Edge Tol. Classes

Fig. 8. 256×256 px Image Comparison

Table 2. Nearness Measures comparison.

Feature	ε	s_r	NM
coef	0.1	any	$\sim$1
cont	0.02	any	1
orien	0	any	0
pos	0.02	any	$\sim$0.05

9.1: Barbara

9.2: Lena

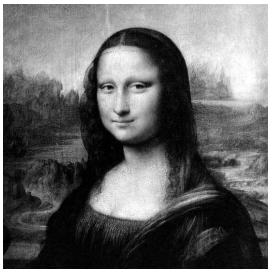

9.3: Mona Lisa

Fig. 9. 512×512 px Portrait Comparison

pends on an epsilon for three different wavelet s_r scales 4, 3 and 2. NM value rises when epsilon value increases. Table 6 presents NMs (12) comparison of contour length for the B & M images. NM values do not depend on epsilon value. Instead, they depend more on scale s_r. All results are presented in Figure 11.1.

4.2.2. B & M comparison

Table 7 presents NMs (12) comparison of contour length for the L & M images. NM values do not depend on the ε value. They more depend on scale s_r. All results are presented in Figure 11.2. Our conclusions are that based on NMs, we are able to state that B & L images are most similar. Other pairs of L & M and B & M are less similar. It is not surprise, because B & L images are real photos, while two last pairs compare the real photo to the painting.

5. Hausdorff and Mahalanobis Distance Measures

In this section, we use the well known Hausdorff and Mahalanobis distance measures.

Table 3. B & L Images Comparison.

wavelet	NM			
s_r	coef	orien	cont	pos
scale	ε=10%	ε=1	ε=10pt	ε=10px
4	0.7830	0.8393	0.7671	0.2777
3	0.7082	0.7148	0.6727	0.2567
2	0.8224	0.7787	0.7222	0.3665
1	0.8928	0.8284	0.7202	0.3062
0		0.5207	0.4762	0.2601

Table 4. B & L NMs for coefficient values.

wavelet	NM (12) based on coefficient					
s_r	epsilon ε					
scale	$\varepsilon = 0$	$\varepsilon = 0.05$	$\varepsilon = 0.1$	$\varepsilon = 0.2$	$\varepsilon = 0.5$	$\varepsilon = 1$
4	0	0.79	0.78	0.78	0.93	0.92
3	0	0.70	0.71	0.72	0.81	0.87
2	0	0.79	0.82	0.84	0.81	0.89
1	0	0.88	0.89	0.90		0.95
0	0	0.46	0.51			

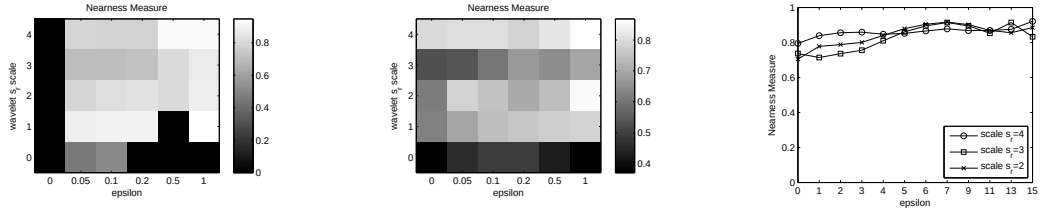

10.1: Coeffient 10.2: Contour 10.3: Orientation

Fig. 10. B & L images NM Measurements Comparison

Algorithm 1: Hausdorff Distance

Input : X, Y (point sets)

Output: *dist* (Hausdorff Distance Measure value)

$dist \leftarrow max(distance(X,Y), distance(Y,X))$;

5.1. Hausdorff Distance Measure

The Hausdorff distance measure [50] inspired by [14, 49] is used to calculate the distance between two point sets $X = \{x_1, x_2, \ldots, x_m\}$ and $Y = \{y_1, y_2, \ldots, y_n\}$ and is defined as

$$d_H(X,Y) = \max(h(X,Y), h(Y,X)), \text{with}, \quad (13)$$

$$h(X,Y) = \max_{x \in X} \min_{y \in Y} \| x - y \|_2, \quad (14)$$

where $\| \cdot \|_2$ is the L_2 norm defined on a point set [12], and where $h(X,Y)$ (14) is called the directed Hausdorff distance (dHd) from X to Y [50]. Geometrically, dHd (14) can be viewed as the radius of the smallest disk that can be drawn about each point of X so that each disk contains at least one point of Y. Using (13), for each point of X, we find its closest neighbour from X and the most mismatched point of X (*i.e.*, the point in X farthest from any point in Y) determines the value of dHd (14).

Table 5. Nearness Measures of B & L images based on contour lengths.

wavelet s_r scale	NM (12) based on contour length, epsilon ε					
	$\varepsilon = 0$	$\varepsilon = 0.05$	$\varepsilon = 0.1$	$\varepsilon = 0.2$	$\varepsilon = 0.5$	$\varepsilon = 1$
4	0.790866	0.803117	0.805671	0.782644	0.821623	0.868421
3	0.533313	0.538091	0.597315	0.672464	0.643665	0.696202
2	0.614586	0.775402	0.747663	0.703257	0.741402	0.856209
1	0.627346	0.691802	0.738488	0.759480	0.772515	0.779761
0	0.372041	0.457141	0.488494	0.490471	0.429877	0.370728

Table 6. Nearness Measures of B & M images based on contour lengths.

wavelet s_r scale	epsilon ε					
	0	0.01	0.05	0.1	0.2	0.3
4	0.5985	0.5985	0.5985	0.6646	0.7027	0.7027
3	0.4945	0.4945	0.5682	0.5434	0.5086	0.4543
2	0.6798	0.6798	0.6896	0.6486	0.6045	0.5995
1	0.6983	0.7627	0.7317	0.6555	0.5851	0.5841
0	0.2394	0.2280	0.2210	0.2241	0.2236	0.2238

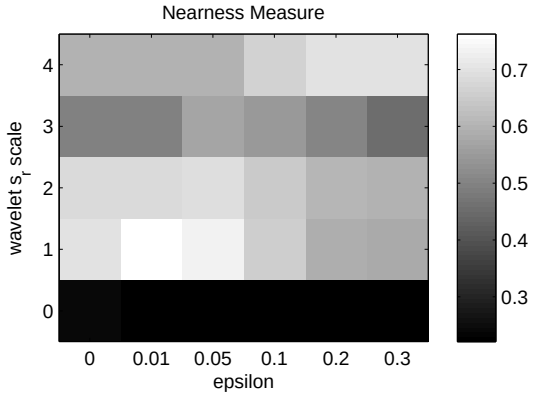

11.1: B & M len.

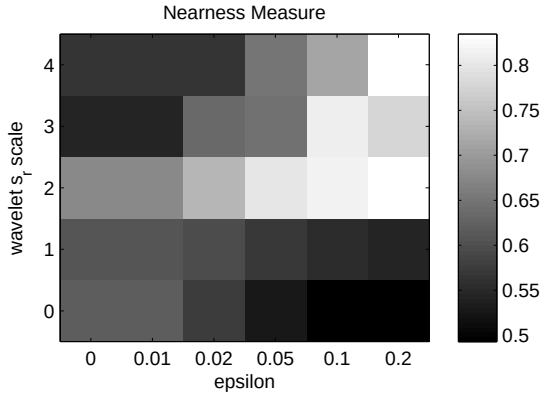

11.2: L & M len.

Fig. 11. Contour Length Comparisons.

Table 7. Nearness Measures of L & M images based on contour lengths.

wavelet s_r scale	epsilon ε					
	0	0.01	0.02	0.05	0.1	0.2
4	0.5631	0.5631	0.5631	0.6504	0.7131	0.8348
3	0.5433	0.5433	0.6331	0.6462	0.8129	0.7799
2	0.6751	0.6751	0.7359	0.7981	0.8182	0.8308
1	0.6054	0.6054	0.5954	0.5697	0.5547	0.5422
0	0.616	0.621	0.5779	0.5274	0.4929	0.4944

Algorithm 2: Directed Hausdorff Distance

Input : A, B (point sets)
Output: $dist$ (distance value)

```
m ← size(A);
n ← size(B);
max ← |A(1) − B(1)|;
for (k ← 1; k < m; k++) do
    min ← A(k) − B(1);
    for (l ← 1; l < n; l++) do
        dist ← |A(k) − B(l)|;
        if dist < min then
            min ← dist;
        end
    end
    if min > max then
        max ← min;
    end
end
dist ← max;
```

5.2. Mahalanobis Distance Measure

We use the Mahalanobis Distance Measure (MDM) [23, 24] to measure dissimilarity between two images. We use features sets X of the first image and Y of the second image. Firstly, we calculate the first image mean values $m_X(i)$ of features $i = \{1,\ldots,n\}$ and their standard deviations $\sigma_X(i)$. We also calculate the second image mean values $m_Y(i)$ and standard deviation $\sigma_Y(i)$ values. Than, we choose the maximum standard deviation $\sigma_{max}(i)$ of each features. At last, we calculate MDM (d_M) of two sets X and Y of image's features as

$$d_M(X,Y) = \sqrt{\sum_{i=1}^{n} \frac{(m_X(i) - m_Y(i))^2}{\sigma_{max}^2(i)}} \,. \qquad (15)$$

This approach was inspired by [7].

6. Image Resemblance Measurement Compared

The results of image resemblance measurements using Hausdorff, Mahalanobis and a nearness measure based on wavelet features, are reported summarized in this section.

Fig. 12.1 presents comparison of similarity measures method based on a wavelet coefficient value feature. NM (12) values distinguish images more than normalized *HDM* (13) and *MDM* (15) values. Fig. 12.2 presents a comparison of similarity measurements based on extracted contour lengths. We normalized the Hausdorff distance measure (13) using with the maximum contour length as a normalizer. NM (12) and normalized *HDM* (13) values are lower than normalized *MDM* (15) values. Fig. 12.3 presents comparison of similarity measures method based on the orientation of extracted edges. *HDM* values are equal to 1 because we use a limited number of orientations (16) and every orientation occurs in both images. normalized *MDM* (15) values are close to 1, which means that using this measure, we would be mislead and conclude that the Lena (L) and Barbara (B) images are almost the same. NM (12) works better because it gives lower values. Fig. 12.4 presents comparison of similarity measurements based on an extracted contours' position (x,y) in the image plane. We normalized Hausdorff Dis-

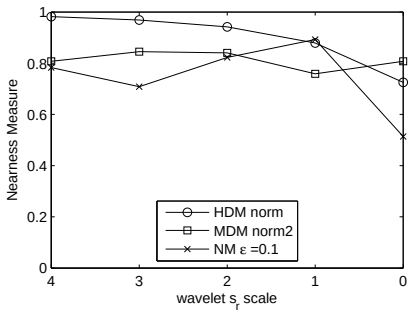

12.1: Coefficient

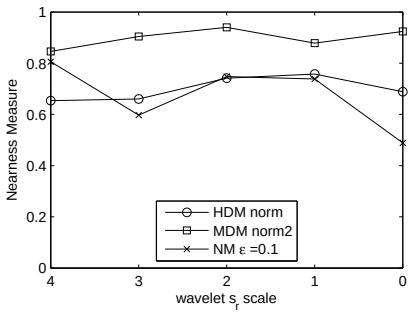

12.2: Contour

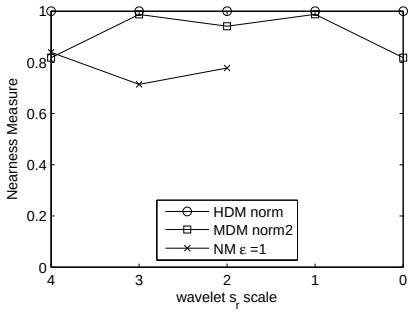

12.3: Orientation

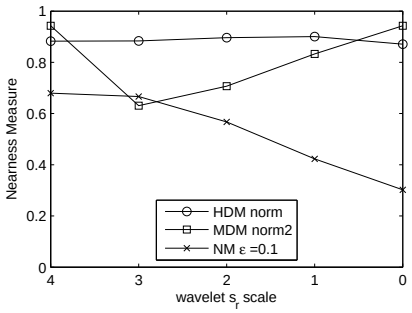

12.4: Position

Fig. 12. Wavelet-Based B & L Images Resemblance Measurements Comparison

tance Measure using the maximum distance, which is equal to the image dimension.

In sum, HDM values based on wavelet coefficient, contour, orientation and position features are about 90%. Again, using the Mahalanobis DM measure, we conclude that the B & L images as almost similar, which does not corespond to our subjective perception. Mahalanobis DM values are in general lower than HDM, but are still higher than NM (12). From the results of the experiments reported in this article and in [6], NM (12) better distinguishes images than either Hausdorff *HDM* (13) or Mahalanobis *MDM* (15) measures in solving the problem of visual recognition of similarities (and dissimilarities) between images.

7. Conclusion

This article presents an anisotropic (direction dependent) wavelet basis for measuring the degree of resemblance between images. Anisotropic wavelets offer a straightforward approach to measuring changes in features of image objects, *e.g.*, object contour lengths (*i.e.*, number of edges belonging to a given contour), spatial orientation, position and wavelet coefficient. Because we want to take into account the differences between image feature values, measures are carried out in an L_2 norm-based perceptual tolerance space. To do this, we use a perceptual tolerance nearness relation $\cong_{\mathscr{B},\varepsilon}$ to establish a framework for image resemblance measurements relative to a chosen set of features $\mathscr{B}$ and a tolerance ε. This is essentially a tolerance near set-based approach to perceiving image resemblance that hearkens back to E.C. Zeeman's 1961 approach to modelling visual perception with tolerances [58]. This approach also has its roots in the original rough set approach to classifying objects *and* perception. Although near sets do not depend on set approximation [44], it is definitely the case that near sets were inspired by a fundamental idea in rough set theory enunciated by E. Orłowska in 1982 [27], namely,

classes in an approximation space serve as a formal counterpart of perception. It is this insight that carries over to classes in a covering defined by a tolerance relation and provides a solid computational intelligence basis for measuring image resemblance. Future work will include the application of the proposed approach in solving image retrieval and video segmentation problems.

Acknowledgements

The authors would like to thank Mirek Pawlak, Piotr Wasilewski, Sheela Ramanna, Andrzej Skowron, Sankar K. Pal, Tony Szturm, Barb Shay, Homa Fashandi, Christopher Henry, Dan Lockery and Amir H. Meghdadi for their insights and suggestions concerning topics in this paper. The authors especially extend their thanks to Christopher Henry for his help in setting up the nearness measure used to compute the measurements reported in this article. This research has been supported by the Natural Sciences & Engineering Research Council of Canada (NSERC) grant 185986, Canadian Arthritis grant SRI-BIO-05, Manitoba Centre for Excellence Fund (MCEF), and Manitoba Hydro grant T277.

1. V. Bruce, P. R. Green, M. A. Georgeson, Visual perception: physiology, psychology, and ecology, Psychology Press, Hove, East Sussex, UK, 1996.
2. E. J. Candès, D. L. Donoho, Curvelets – a surprisingly effective nonadaptive representation for objects with edges (1999).
   URL `http://www-stat.stanford.edu/~donoho/Reports/1999/curveletsurprise.pdf`
3. E. J. Candès, D. L. Donoho, New tight frames of curvelets and optimal representations of objects with piecewise-c2 singularities., Comm. Pure Appl. Math. 57 (2002) 219–266.
4. M. N. Do, M. Vetterli, The contourlet transform: an efficient directional multiresolution image representation, IEEE Transactions on Image Processing 14 (12) (2005) 2091–2106.
5. G. Brunner, Structure features for content-based image retrieval and classification problems, Ph.d. diss., Albert-Ludwigs-Universität Freiburg (2006).
6. H. Fashandi, J. Peters, S. Ramanna, l_2 norm length-based image similarity measures: Concrescence of image feature histogram distances, Signal and Image Processing, (2009), *in press*.
7. J. Angulo, J. Serra, Morphological color size distribution for image classification and retrieval, in: Proc. Advanced Concepts for Intelligent Vision Systems, Ghent, Belgium, 2002.
8. T. Deselares, Features for image retrival, Phd diss., Rheinisch-Westfalische Technische Hochschule Aachen (2003).
9. W. Bartol, J. Miró, K. Pióro, F. Rosselló, On the coverings by tolerance classes, Inf. Sci. Inf. Comput. Sci. 166 (1-4) (2004) 193–211.
10. M. Geetha, S. Palanivel, Video classification and shot detection for video retrieval applications, International Journal of Computational Intelligence Systems 2 (1) (2009) 39–50.
11. S. N. Gerasin, V. V. Shlyakhov, S. V. Yakovlev, Set coverings and tolerance relations, Cybernetics and Sys. Anal. 44 (3) (2008) 333–340.
12. C. Gope, N. Kehtarnavaz, Affine invariant comparison of point-sets using convex hulls and hausdorff distances, Pattern Recogn. 40 (1) (2007) 309–320.
13. A. E. Hassanien, A. Abraham, J. F. Peters, G. Schaefer, C. Henry, Rough sets and near sets in medical imaging: A review, IEEE Transactions on Information Technology in Biomedicine (2009) digital object identifier:10.1109/TITB.2009.2017017, in press.
    URL `http://ieeexplore.ieee.org/xpl/tocpreprint.jsp?isnumber=4358869&punumber=4233`
14. F. Hausdorff, Dimension und äusseres mass, Math. Ann. 79 (1919) 157–179.
15. C. Henry, J. Peters, Near set evaluation and recognition (near) system, Tech. rep., Computationa Intelligence Laboratory, University of Manitoba, UM CI LABORATORY TECHNICAL REPORT No. TR-2009-015 (2000).
    URL `http://wren.ee.umanitoba.ca/images/ci\_reports/reportci-2009-015.pdf`
16. C. Henry, J. Peters, Perception-based image analysis, Int. J. of Bio-Inspired Computation 2 (2), *in press*.
17. C. Henry, J. F. Peters, Image pattern recognition using approximation spaces and near sets, in: Proc. of the Eleventh International Conference on Rough Sets, Fuzzy Sets, Data Mining and Granular Computer (RSFDGrC 2007), Joint Rough Set Symposium (JRS07), Lecture Notes in Artificial Intelligence, vol. 4482, 2007.
18. C. Henry, J. F. Peters, Near set index in an objective image segmentation evaluation framework, in: GEOgraphic Object Based Image Analysis: Pixels, Objects, Intelligence, University of Calgary, Alberta, 2008.
19. C. Henry, J. F. Peters, Near sets, Wikipedia.
    URL `http://en.wikipedia.org/wiki/Near_sets`
20. J. Ilonen, Supervised local image feature detection, Phd diss., Lappeenrannan teknillinen yliopisto, Lappeenranta (2007).
21. K. Jänich, Topology, Springer-Verlag, Berlin, 1984.
22. J. Kämäräinen, Feature extraction using gabor filters, Phd diss., Lappeenrannan teknillinen yliopisto, Lappeenranta (2003).
23. P. Mahalanobis, On tests and measures of group divergence i. theoretical formulae, J. and Proc. Asiat. Soc. of Bengal 26 (1930) 541–588.

24. P. Mahalanobis, On the generalized distance in statistics, Proc. Nat. Institute of Science (Calcutta) 2 (1936) 49–55.
25. S. G. Mallat, A Wavelet Tour of Signal Processing, Academic Press, 1999.
26. A. Meghdadi, J. Peters, S. Ramanna, Tolerance classes in measuring image resemblance, Intelligent Analysis of Images & Videos, (2009), *in press*.
27. E. Orłowska, Semantics of vague concepts. applications of rough sets, Tech. Rep. 469, Institute for Computer Science, Polish Academy of Sciences (1982).
28. E. Orłowska, Semantics of vague concepts, in: G. Dorn, P. Weingartner (eds.), Foundations of Logic and Linguistics. Problems and Solutions, Plenum Pres, London/NY, 1985, pp. 465–482.
29. M. Pavel, Fundamentals of Pattern Recognition, 2nd ed., Marcel Dekker, Inc., N.Y., U.S.A., 1993.
30. Z. Pawlak, Classification of objects by means of attributes, Tech. Rep. PAS 429, Institute for Computer Science, Polish Academy of Sciences (1981).
31. Z. Pawlak, Rough sets, International Journal of Computer and Information Sciences 11 (1982) 341–356.
32. Z. Pawlak, J. Peters, Jak blisko (how near), Systemy Wspomagania Decyzji I (2002,2007) 57,109.
33. Z. Pawlak, A. Skowron, Rudiments of rough sets, Information Sciences 177 (2007) 3–27.
34. J. Peters, Classification of objects by means of features, in: Proceedings of the IEEE Symposium Series on Foundations of Computational Intelligence (IEEE SCCI 2007), Honolulu, Hawaii, 2007.
35. J. Peters, Near sets. general theory about nearness of objects, Applied Mathematical Sciences 1 (53) (2007) 2609–2629.
36. J. Peters, Near sets. special theory about nearness of objects, Fundamenta Informaticae 76 (2007) 1–27.
37. J. Peters, Classification of perceptual objects by means of features, Int. J. of Info. Technology & Intell. Computing 3 (2) (2008) 1–35.
38. J. Peters, Discovery of perceptually near information granules, in: J. T. Yao (ed.), Novel Developements in Granular Computing: Applications of Advanced Human Reasoning and Soft Computation, Information Science Reference, Hersey, N.Y., USA, 2009, p. in press.
39. J. Peters, Tolerance near sets and image correspondence, Int. J. of Bio-Inspired Computation 4 (1) (2009) 239–445.
40. J. Peters, L. Puzio, Measuring nearness of rehabilitation hand images with finely-tuned anisotropic wavelets, in: 1^{st} Int. Conf. on Image Processing & Communications, Bydgoszcz, Poland, 2009.
41. J. F. Peters, Fuzzy sets, near sets, and rough sets for your computational intelligence toolbox, in: A.-E. Hassanien, A. Abraham, F. Herrera (eds.), Foundations of Computational Intelligence, Volume 2, Approximate Reasoning Series: Studies in Computational Intelligence, Vol. 202, Springer-Verlag, Berlin, 2009, iSBN: 978-3-642-01532-8.
42. J. F. Peters, L. Puzio, T. Szturm, Measuring nearness of rehabilitation hand images with finely-tuned anisotropic wavelets, Int. Conf. on Image Processing & Communication (2009) submitted.
43. J. F. Peters, S. Ramanna, Affinities between perceptual granules: Foundations and perspectives, in: A. Bargiela, W. Pedrycz (eds.), Human-Centric Information Processing Through Granular Modelling, Springer-Verlag, Berlin, 2008, pp. 49–66.
44. J. F. Peters, P. Wasilewski, Foundations of near sets, Information Sciences. An International Journal (2009) digital object identifier: doi:10.1016/j.ins.2009.04.018, in press. URL `http://dx.doi.org/10.1016/j.ins.2009.04.018`
45. H. Poincaré, The topology of the brain and the visual perception, Prentice Hall, New Jersey, 1965, in K.M. Fort, Ed., Topology of 3-manifolds and Selected Topics, 240-256.
46. L. Puzio, Adaptive edge extraction method for images, Ph.D. thesis, Military University of Technology in Warsaw (2008).
47. L. Puzio, A. Walczak, 2-d wavelet with position controlled resolution, in: Medical Imaging, vol. 5959, SPIE, Warsaw, 2005.
48. L. Puzio, A. Walczak, Adaptive edge detection method for images, Opto-Electronics Review 16 (1) (2008) 60–67.
49. C. Rogers, Hausdorff Measures, Cambridge, UK, Cambridge U Press, 1970.
50. W. Rucklidge, Efficient Visual Recognition Using the Hausdorff Distance, Springer-Verlag, Berlin, 1996.
51. C. Sanderson, K. Paliwal, Fast feature extraction method for robust face verification, Electronics Letters 38 (25) (2002) 1648–1650.
52. M. Schroeder, M. Wright, Tolerance and weak tolerance relations, Journal of Combinatorial Mathematics and Combinatorial Computing 11 (1992) 123–160.
53. Y. A. Shreider, Tolerance spaces, Cybernetics and Systems Analysis 6 (12) (1970) 153–758.
54. A. Skowron, J. Stepaniuk, Tolerance Approximation Spaces, Fundamenta Informaticae 27 (2/3) (1996) 245–253.
55. A. Sossinsky, Tolerance space theory and some applications, Acta Applicandae Mathematicae: An International Survey Journal on Applying Mathematics and Mathematical Applications 5 (2) (1986) 137–167.
56. V. Velisavljevic, B. Beferull-Lozano, M. Vetterli, P. L. Dragotti, Directionlets: Anisotropic Multidirectional representation with separable filtering, IEEE Transactions on Image Processing 15 (7) (2006) 1916–1933.
57. V. D. Witte, S. Schulte, E. Kerre, New vector ordering in the redgreenblue colour model with application to morphological image magnification, International Journal of Computational Intelligence Systems 1 (2) (2008) 103–115.
58. E. Zeeman, The topology of the brain and the visual perception, Prentice Hall, New Jersey, 1965, in K.M. Fort, Ed., Topology of 3-manifolds and Selected Topics, 240-256.
59. Z. Zheng, H. Hu, Z. Shi, Tolerance Relation Based Granular Space, Lecture Notes in Computer Science 3641 (2005) 682.